Progress in Additive Manufacturing
https://doi.org/10.1007/s40964-026-01570-6

RESEARCH

3D printed multifunctional transparent composites of cellulose nanocrystal and graphene quantum dot aerogels

Halil Tetik[1,2] · Darwin Kurniawan[3] · Guang Yang[4,2] · Yisheng Sun[5] · Licong An[6] · Mahya Rahbar[7] · Gary J. Cheng[6] · Caixia Wan[5] · Xinwei Wang[7] · Wei-Hung Chiang[3] · Dong Lin[8,2]

Received: 10 June 2025 / Accepted: 29 January 2026

Abstract
The conventional top-down approach used for the fabrication of transparent wood composites comes with certain issues including the use of excess chemicals, limited patternability of the optical properties, and requirement of natural trees as the raw material. Here, we propose a novel bottom-up approach where we start with cellulose nanocrystals, which can be obtained either from trees or other eco-friendly resources such as grass, and bacterial cellulose. Our 3D printed cellulosic aerogels have a microstructure similar as the delignified wood used in the conventional fabrication process and demonstrate a high optical transparency (87%). Furthermore, incorporating 3D printing enables precise patterning of the material so that we can achieve patterned optical transparency. We further functionalized our ink using nitrogen doped graphene quantum dots and fabricated multifunctional composites with patterned UV illumination properties with an ability to precisely measure the temperature. Our approach is a promising method for cost-efficient fabrication of optical devices for applications such as gradient refractive index lenses, smart windows, and screens.

Keywords Multifunctional transparent wood · 3D printed cellulose aerogel · Graphene quantum dot · 3D freeze printing

✉ Halil Tetik
haliltetik@iyte.edu.tr

✉ Dong Lin
dong.lin@oregonstate.edu

Darwin Kurniawan
jdkywt@gmail.com

Guang Yang
gyang@ksu.edu

Yisheng Sun
ys3h2@mail.missouri.edu

Licong An
alc0127@hotmail.com

Mahya Rahbar
mrahbar@iastate.edu

Gary J. Cheng
gjcheng@purdue.edu

Caixia Wan
wanca@missouri.edu

Xinwei Wang
xwang3@iastate.edu

Wei-Hung Chiang
whchiang@mail.ntust.edu.tw

[1] Mechanical Engineering Department, Izmir Institute of Technology, Izmir, Turkey

[2] Industrial and Manufacturing Systems Engineering Department, Kansas State University, Manhattan, USA

[3] Department of Chemical Engineering, National Taiwan University of Science and Technology, Taipei, Taiwan

[4] Manufacturing and Materials Research Laboratories, Purdue University, West Lafayette, USA IN

[5] Department of Chemical and Biomedical Engineering, University of Missouri, Columbia, USA

[6] School of Industrial Engineering, Purdue University West Lafayette, West Lafayette, USA

[7] Department of Mechanical Engineering, Iowa State University, Ames, USA

[8] Mechanical, Industrial, and Manufacturing Engineering Department, Oregon State University, Corvallis, USA

Published online: 26 February 2026

1 Introduction

Wood, which is one of the most important structural materials obtained from natural and renewable sources, has been widely used due to its excellent mechanical properties [1, 2]. In 1992, when Siegfried Fink proposed transparent wood (TW) as an example of multifunctional wood composites [3], a light management functionality to the excellent load-bearing properties of natural wood was added [4]. As presented in Fig. 1a, the conventional top-down approach for TW fabrication starts with the delignification of the natural wood, then a polymer with a matching refractive index (η) is infiltrated into the pores of the delignified wood to achieve an optical transparency [5]. Cellulose and lignin constitute the main composition of the natural wood where cellulose provides the structural strength, and lignin acts as cementing agent which binds cellulose together [6]. Lignin, which is responsible for 80–95% of the light absorption in natural wood is removed with the delignification process [7]. The highly ordered porous cellulose structure that remains after delignification has a white color due to light scattering caused by the refractive index mismatch between the cellulosic walls ($\eta \approx 1.53$) and the air ($\eta \approx 1$) filling the pores. When the pores are filled with a polymer having a matching refractive index such as Poly(methyl methacrylate) (PMMA - $\eta \approx 1.49$), epoxy ($\eta \approx 1.5$) and Polyvinylpyrrolidone (PVP - $\eta \approx 1.53$), the scattering of the light is minimized and an optical transparency is obtained [4].

Incorporating a top-down approach for the fabrication of TW and its multifunctional composites is an effective way, however, the solution-based delignification process consumes large amounts of chemicals and energy. Besides, due to the nature of the fabrication process, it is not possible to achieve a freedom in the design where the optical transparency can be geometrically patterned. To the best of our knowledge, the only exception to this inevitable situation is a study performed by the research group of Dr. Hu from the University of Maryland [8]. In their study, they incorporated a solar assisted chemical brushing method to remove the lignin chromophore content which is responsible for brownish color and light absorption properties of natural wood. They modified the lignin structure by brushing it with H_2O_2 across the wood surface and exposed it to the sunlight. The UV illumination from the natural sunlight removed the light-absorbing chromophores of lignin and with the epoxy infiltration, the TW was obtained. Simply by selective chemical assisted brushing, TW having patterns with designed optical transparency were obtained. Although their method requires fewer chemicals and energy consumption; and provides a design freedom in two dimensions, it is still a top-down approach where a design freedom in three dimensions is not possible. Furthermore, the raw material still needs to be natural wood obtained from trees, which hinders the use of alternative and eco-friendly cellulose resources such as cellulose from grass or bacterial cellulose [9].

Upgrading TW with various multifunctionalities has been a common research interest and proposed by different research groups. Multifunctional TW was usually achieved by mostly doping the polymer matrix with different functional nanoparticles. One of the earliest works that reports multifunctional TW involved doping the polymer matrix with silicon quantum dots (QD) before infiltration of the delignified wood so that the TW would achieve a diffused luminescence without optical degradation [10]. Wang et al. proposed infiltrating the delignified wood with a mixture of a photochromic material and matrix polymer so that the fabricated TW exhibits a vibrant purple-to-colorless color change with the exposure light for smart window applications [11]. Incorporating UV absorbing agents [12], or trace amount of lignin nanoparticles [13] in the polymer matrix composition provided TW a significant UV shielding capability. In another study, PMMA matrix doped with Cs_xWO_3 nanoparticles was used to fabricate TW, and Cs_xWO_3 nanoparticles provided an excellent near-infrared shielding ability without compromising the visible light transparency for smart window applications [14]. It is also possible to dope the delignified wood with the functional material before the polymer infiltration to achieve multifunctionality. One example of such case was proposed by Montanari et al., where they encapsulated phase change materials into the delignified wood substrate to store the thermal energy for energy efficient building applications [15]. Yet, for all of these multifunctional TWs, it is not possible to achieve a precise patterning of the functional dopant since they are obtained after a top-down fabrication approach which doesn't allow any freedom of design.

None of the previously reported top-down approaches have addressed the need for scalable, design-flexible, and multifunctional TW fabrication. Hence, here in this work, we employ a novel bottom-up approach for the fabrication of multifunctional transparent wood composites where we address the design freedom issues by employing inkjet 3D printing technology. Our fabrication procedure starts with 3D freeze printing (3DFP) of cellulose nanocrystal (CNC) aerogels. The microstructure of our 3D printed CNC aerogels resembles the microstructure of the delignified wood used in the conventional top-down fabrication of TWs. Then, 3D printed aerogels with different average pore sizes, which were controlled by the solid loading in the ink formulation, were infiltrated with clear epoxy and we achieved a high optical transmission that can reach up to ~85%. The average pore size helped to control the level of epoxy infiltration, which eventually helped us to tune the optical transparency of the final TW composites. By incorporating

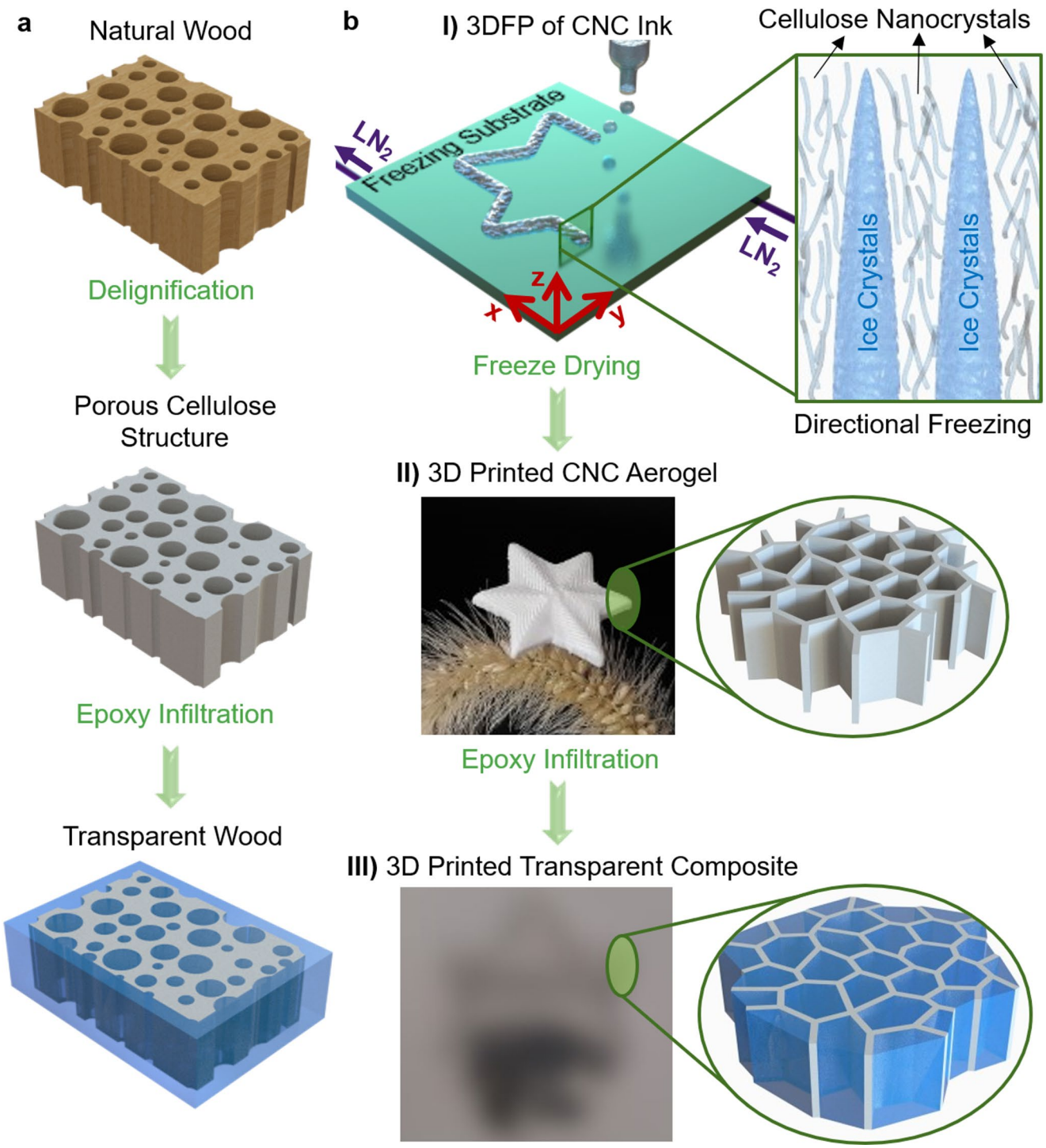

Fig. 1 Schematic illustration showing the conventional and proposed fabrication procedures. (**a**) Conventional top-down fabrication process of transparent wood. Natural wood first is delignified, and the obtained porous cellulose structure is infiltrated with a polymer having a matching refractive index. (**b**) Proposed bottom-up approach. CNC ink is selectively deposited by an inkjet head on top of a freezing substrate to obtain 3D printed frozen structures. Subsequently applied freeze-drying results in CNC aerogels with an aligned microstructure. Infiltrating epoxy yields to 3D printed TCs with tunable transparency (Anonymized)

multiple print-heads loaded with different inks, we were able to achieve transparent composites (TCs) with programmed and heterogenous optical transparency were obtained. While our transparent composites are comparable with TW in terms of their optical transparency along the freezing direction and mechanical properties, the anisotropy

conventionally observed in TW was not investigated due to the limited sample dimensions that we can achieve along the freezing direction using our current experimental setup. Furthermore, we used graphene quantum dots (GQDs) as multifunctional additives in the ink formulation which provided a functionality for temperature measurements. Proposed bottom-up fabrication strategy for the transparent wood composites has great potential to eliminate waste generation which will be unavoidable when TW with certain geometries needs to be fabricated; and decorating them with a wide range of dopants with precisely controlled location of the dopants on the TW body. Our bottom-up approach for achieving TCs and ability to use different additives reveals a great potential for cost-effective fabrication of multifunctional TCs and optical devices such as gradient refractive index lenses and smart windows.

2 Materials and methods

2.1 NGQD synthesis

Briefly, 300 mg of chitosan (low molecular weight, 50–190 kDa, Sigma Aldrich, MO, USA) was dissolved in 40 mL of 50 mM acetic acid (MI, USA). 10 mL of chitosan solution was then subjected to a microplasma treatment at a fixed discharge current of 9.6 mA for 60 min to synthesize the NGQDs. Afterwards, the plasma treated solution was neutralized with 1 M NaOH and added with 20 mL of acetone to precipitate the unreacted chitosan. The precipitate and acetone were subsequently removed by vacuum filtration and rotary evaporation. Then, the obtained solution was dialyzed (Biotech CE Tubing, 500–1000 Da, Spectrum Laboratories, Taipei, Taiwan) against DI water for 2 days. The outer solution was replaced with fresh DI water every 6 h. Finally, the solution inside the dialysis bag was evaporated using rotary evaporator to obtain fine NGQD powder.

2.2 3DFP of CNC and CNC+NGQD aerogels

CNC powder was purchased from Celluforce (Quebec, Canada) and used as delivered. For the synthesis of aqueous CNC ink, we mixed CNC powder with DI water to achieve desired ink concentration via a mechanical stirring process. For the 3D freeze printing of CNC aerogels, a three-axis motion stage (Panowin Technologies, Shanghai, China) was used to manipulate the DOD print-head, which was composed of a syringe barrel (Nordson EFD, RI, USA) and a solenoid micro dispenser (The Lee Co, CT, USA) loaded with a nozzle tip having a diameter of 130 μm. Desired inks were loaded inside the syringe barrel and the pressure was controlled using a pneumatic fluid dispenser (Nordson EFD, RI, USA). Droplets of the inks were generated by the inkjet dispenser, and they were deposited on to the freezing substrate whose temperature was controlled by a liquid nitrogen ($L-N_2$) operated hot/cold plate (Instec, CO, USA). Frozen constructs were freeze-dried at −35°C and 0.2 mbar for 48 h to achieve CNC aerogels by using a commercial benchtop freeze dryer (Labconco, MO, USA).

2.3 Epoxy infiltration

The epoxy resin (#300) and curing agent (#21) was purchased from Aeromarine Products Inc. (CA, USA), and mixed with 2:1 weight ratio according to the manufacturer's directions. 3D printed CNC aerogels were placed inside lab designed and 3D printed PLA cages and dipped into the epoxy-curing agent mixture. The cage helped to protect the shape and structural integrity of the aerogels during the infiltration process under high vacuum. During the 3DFP process, we have used inks having three different solid loading values: 2, 3.5, and 5 wt%, which was enforced by the printability requirements of inkjet printing technology employed for the 3D freeze printing process. Then, TCs obtained after epoxy infiltration have been named as TC2, TC3.5 and TC5 based on the initial solid loading of the used ink.

2.4 Characterizations

The microstructure of the 3DFP aerogels was investigated by SEM (FEI HELIOS Nanolab 600i, OR, USA). Light transmittance was recorded on a UV–Vis spectroscopy (Lambda 35, PerkinElmer Inc., Waltham, MA, USA) from 800 to 400 nm. For tensile and 3-point-bending compression tests, a digital material testing device (Shimadzu Universal Testing Machine, Kyoto, Japan) was used. For the tensile tests, five samples having 3 mm thickness and 15 mm gage length has been prepared for each group. For the 3-point-bending compression tests, five samples with the dimensions of 5 × 50 × 3 mm were prepared for each group. Both tensile and flexural tests have been performed using 5 $mm.min^{-1}$ strain rate. The out-of-plane thermal conductivity of the pure epoxy and TC samples was measured using the differential thermal resistance (DTR) technique [16]. This technique, which has been tested and validated with an uncertainty better than 5% by measuring thermal conductivity of acrylic and glass slide samples, ensures reliable results. In the DTR technique, as presented in Figure S1a, a double-sided black tape was used to coat the sample and attach it to an aluminum (Al) substrate. A continuous wave laser with a wavelength of 1550 nm (which is out of the range of sensing wavelength of the infrared camera 8–14 μm in order not to affect the temperature measurements) irradiated the top surface of the black tape, while an infrared camera measured the resulting

surface temperature rise. This temperature rise (ΔT) for the sample case depends on the absorbed laser power (Q), the thermal resistance of radiation-convection (R_{rc}), the thermal resistance of the two black tapes (R_t), the thermal resistance of the sample (R_s), and the thermal resistance of the substrate (R_{sub}). The thermal resistance circuit for the sample case is also presented in Figure S1a. The top black tape was used to maximize laser absorption and minimize reflection, and the Al substrate ensured efficient heat dissipation from the sample. Furthermore, the laser spot covered the entire sample to ensure uniform heating, and the laser power was measured precisely with a power meter. To account for several unknowns, including the thermal resistance of black tapes, Al substrate, and radiation-convection, two additional cases were designed. The first one was a reference case, which is a 1-mm glass slide with known thermal conductivity (k_g = 1.27 W·(m·K)$^{-1}$), as presented in Figure S1b. The other case involved two layers of double-sided black tape, identical to those used in the sample case, as presented in Figure S1c. The reference case closely resembles the sample case, but the sample has been replaced with a glass slide. The same laser and infrared camera were also used for all three cases, each with a cross-sectional area of 8 × 8 mm^2.The thermal resistance circuits shown in Figure S1 led to the following equations:

$$Q_s = \Delta T_s \left[\frac{1}{R_{rc}} + \frac{1}{R_{tot} + R_s} \right] \tag{1}$$

$$Q_g = \Delta T_g \left[\frac{1}{R_{rc}} + \frac{1}{R_{tot} + R_g} \right] \tag{2}$$

$$Q_{tot} = \Delta T_{tot} \left[\frac{1}{R_{rc}} + \frac{1}{R_{tot}} \right] \tag{3}$$

where the subscript s, g, and tot represent the sample, the glass slide, and the combination of the two black tapes and Al substrate, respectively. By solving Eqs. (1–3), the sample's thermal resistance can be determined, which can then be converted to the sample's thermal conductivity using $k_s = t_s / R_s A_s$. Here, the t_s and A_s are the sample's thickness, obtained using a digital micrometer, and the cross-sectional area (8 × 8 mm^2). The experimental details for thermal conductivity measurements of pure epoxy, with a measured thickness of 2.6 mm, and the TC2 sample, with a measured thickness of 2.2 mm, are presented in Table S1. Note that T_1 and T_2 represent the temperature of cases before and during laser irradiation, and ΔT is the temperature rise caused by the laser irradiation. It should also be noted that in the DTR technique, only the relative temperature change is of interest rather than the absolute temperature rise. Therefore, any systematic error in absolute temperature measurement by the infrared camera will be ruled out during temperature change determination.

PL measurements of colloidal NGQD were performed at room temperature using a commercial spectrometer (Horiba JobinYvon Nanolog-3 spectrofluorometer, Kyoto, Japan) equipped with an InGaAs NIR detector and a 20 nm bandpass for both emission and excitation. MicroRaman measurement was conducted at room temperature with a JASCO 5100 spectrometer (Tokyo, Japan) with a laser excitation wavelength of 532 nm. TEM measurements were performed using a field emission gun TEM (JEOL JEM-2100 F, Tokyo, Japan) with an accelerating voltage of 200 kV. TEM samples were prepared from solution dry-casting of the colloidal NGQD onto pure carbon-coated copper grids (400 mesh, Ted Pella Inc., CA, USA). PL-based temperature sensing was performed using a Horiba JobinYvon Nanolog-3 spectrofluorometer (Kyoto, Japan) equipped with a controllable temperature water bath flowing through the sample chamber. All the solid state measurements were conducted in a front face mode, and the sample chamber was located at 0° from the excitation source. I_0 and I represent the PL intensities measured at 25 °C and different temperatures, respectively. The measurements were conducted for three times.

3 Results and discussion

The fabrication process of our TCs using a bottom-up approach starts with mixing the commercially available CNC powder with DI water to obtain the ink. By adjusting the CNC solid loading, the rheology of the ink as well as the final microstructure can be engineered. In order maintain the printability of the ink, we kept the maximum solid loading at 5 wt%. To ensure the structural integrity of the CNC aerogels during the epoxy infiltration, we kept the minimum solid loading at 2 wt%. Hence, we performed our experiments with three different solid loading values: 2, 3.5, and 5 wt%, and named our TCs based on the solid loading of the ink (i.e., the TC obtained from 3.5 wt% ink is named TC3.5, etc.). As presented in Fig. 1b-I, once the ink is simply prepared by magnetic stirring of weighted amount of CNC in DI water at room temperature, ink is then loaded into an inkjet head setup attached to a 3D printing platform. As the droplets of the ink are generated and selectively deposited on top of a freezing substrate, they immediately freeze and preserve their shape. By adjusting the time lapse and distance between the successive droplets, we obtained uniform frozen lines. Throughout the freezing of the ink, ice crystals nucleate on the substrate and grow along the freezing direction as in unidirectional freeze casting. Growing ice crystals tightly stack the CNCs and the subsequently applied freeze-drying step results in a porosity that is a

replica of the developed ice crystals (Fig. 1b-II). Hence, the unidirectional growth of ice crystals helps us to obtain a highly ordered porosity resembling the microstructure of the delignified wood. After obtaining CNC aerogels following the freeze-drying step, the clear epoxy is well-infiltrated into pores which leads to a highly transparent composites as presented in Fig. 1b-III. As the TCs are fabricated from 3D printed CNC aerogels, the shape of those can be precisely manipulated to obtain cost-efficient functional devices such as optical lenses as presented in Figure S2. Enabling the fabrication of such 3-dimensional transparent composites further extends the work of Xia et al., where they have used a solar assisted patternable transparency for conventional TWs.

Due to the unidirectional freezing employed in 3DFP method, the microstructure of the obtained aerogels has highly anisotropic nature where the pores and cellulose walls are aligned along the freezing direction. As seen in the cross-sectional micrograph presented in Fig. 2a, the alignment of the microstructure along the freezing direction (shown with the white arrow) resembles the microstructure of the delignified wood that is used for the fabrication of TW using the conventional top-down approach [2]. When the 3D printed CNC aerogels further infiltrated with epoxy, the highly ordered microstructure along the freezing direction is preserved (Figure S3). Tuning the solid loading of the precursor solution to engineer the final product's microstructure as well as materials properties has been commonly employed during the conventional unidirectional freeze casting process [17–19]. As the solid loading increases the average size of the pores decreases in freeze casting processes. The same applies to the 3DFP process. As the ink solid loading increases from 2 to 5 wt%, the pores seen in the micrographs gets smaller (Fig. 2b-d).

Decreasing the average size of the pores impedes the infiltration of epoxy into the pores, which greatly affects the optical properties of the TCs. Hence, the transmittance of TC2 reaches up to ~ 87% while the transmittance values remain at ~ 86 and ~ 82% for TC3.5 and TC5, respectively (Fig. 2e). The difference between the optical transmittance of the samples can be better observed with the actual samples presented in Figure S4. It should be noted that the optical transmittance of TC2 sample is only 1% lower than bare epoxy showing that almost all the pores available in the microstructure of the 3D printed aerogels were filled with epoxy. To further investigate the effect of sample thickness, we have fabricated TC2 samples with varying thickness values (Fig. 2f). While the transmittance of 1- and 2-mm thick samples remained at ~ 87%, the 3 mm sample had a transmittance of ~ 83%. All these samples were fabricated in a monolithic fashion with uniform optical properties. However, as previously reported by Xia et al., TWs with

Fig. 2 Structural and optical properties of 3D printed CNC aerogels and TCs. (**a**, **b**) Cross-sectional and top view SEM images showing the microstructure of 3D printed CNC aerogels with highly ordered anisotropic nature. c-d) Top view (parallel to the freezing direction) of the 3D printed CNC aerogels made from 3.5 and 5 wt% solid loading ink. (**e**) Optical transmittance of pure epoxy, TC2, TC3.5 and TC5 having 2 mm sample thickness. f) Optical transmittance of the TC2 with varying thickness. g) Demonstration of a TC composite with patterned optical transparency (Anonymized)

patternable transparency is required for precise guiding of the light [8]. Unlike their work where they selectively delignify natural wood by brushing it, here we selectively deposit the CNC inks with different solid loading values to fabricate one single TC sample. This helped us to precisely locate different optical properties on TC samples to achieve a precise guidance of the light. As presented in Fig. 2g, our method enabled us to fabricate TCs with patterned optical transparency values. Our method's ability to precisely pattern the optical transparency can enable cost efficient fabrication of optical devices for various applications such as gradient refractive index lenses and smart windows.

The mechanical properties of conventional TWs fabricated by top-down approach are usually compared with natural wood, infiltrated polymer and sometimes glass since they are usually offered as alternative to glass in buildings. Due to the anisotropic nature of the TW, characterization of the tensile properties is usually performed in two directions: longitudinal (force being applied parallel to the cellulose wall alignment), and tangential (force being applied perpendicular to the cellulose wall alignment) [1, 2]. The tensile properties of our TCs were characterized in tangential direction. As presented in Fig. 3a, the elastic modulus (E) of our TC2 sample showed a ~ 21% increase compared to the infiltrated polymer, epoxy. On the other hand, its tensile strength was ~ 22% lower. The strain at break (ε) values were measured as 4.93% for pure epoxy and 2.67% for TC2. These trends in the tensile properties of our samples are similar with the results of Li et al., where the authors compared the tensile properties of TWs with the infiltrated polymer (poly(methyl methacrylate) (PMMA)) in both directions [1]. Besides, the measured values of E and σ for TC2 are in a good agreement with the findings of Zhu et al., where they reported the mechanical properties of TWs fabricated from very same infiltrated polymer [2]. We further characterized the mechanical properties of our TCs by 3-point-bending tests and compared their performance with the infiltrated epoxy. As presented in Fig. 3b, the 3-point-bending tests revealed ~ 29% increase in the flexural modulus of TC2 compared to pure epoxy while the flexural strength decreased by ~ 16%. A similar comparison in the flexural modulus and strength of the TW and infiltrating polymer has been previously reported by Li et al. [20]. While the increase in the flexural modulus has a similar trend, they observed an

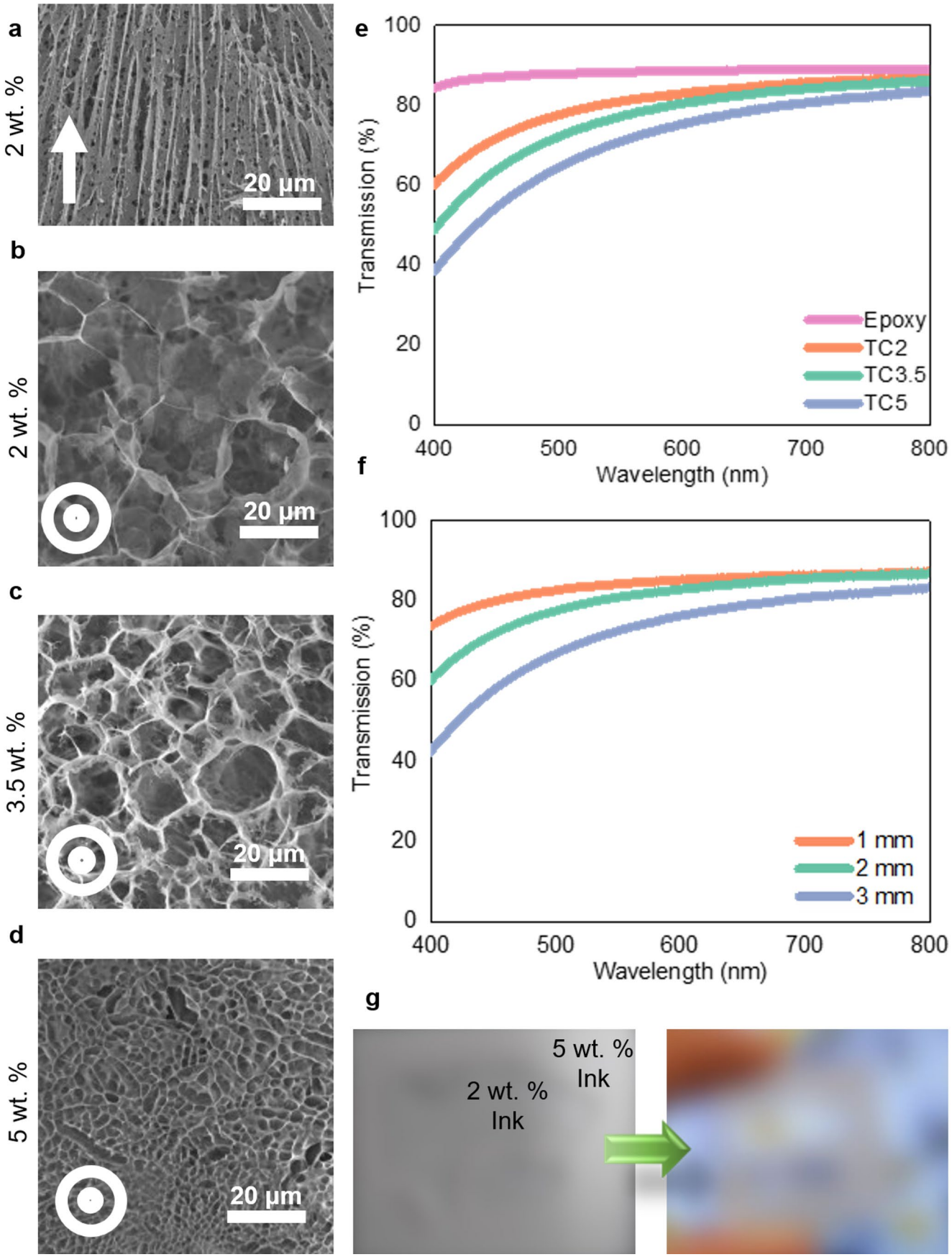
a
2 wt. %
20 μm
b
2 wt. %
20 μm
c
3.5 wt. %
20 μm
d
5 wt. %
20 μm
e
Transmission (%)
Wavelength (nm)
Epoxy
TC2
TC3.5
TC5
f
Transmission (%)
Wavelength (nm)
1 mm
2 mm
3 mm
g
2 wt. %
Ink
5 wt. %
Ink

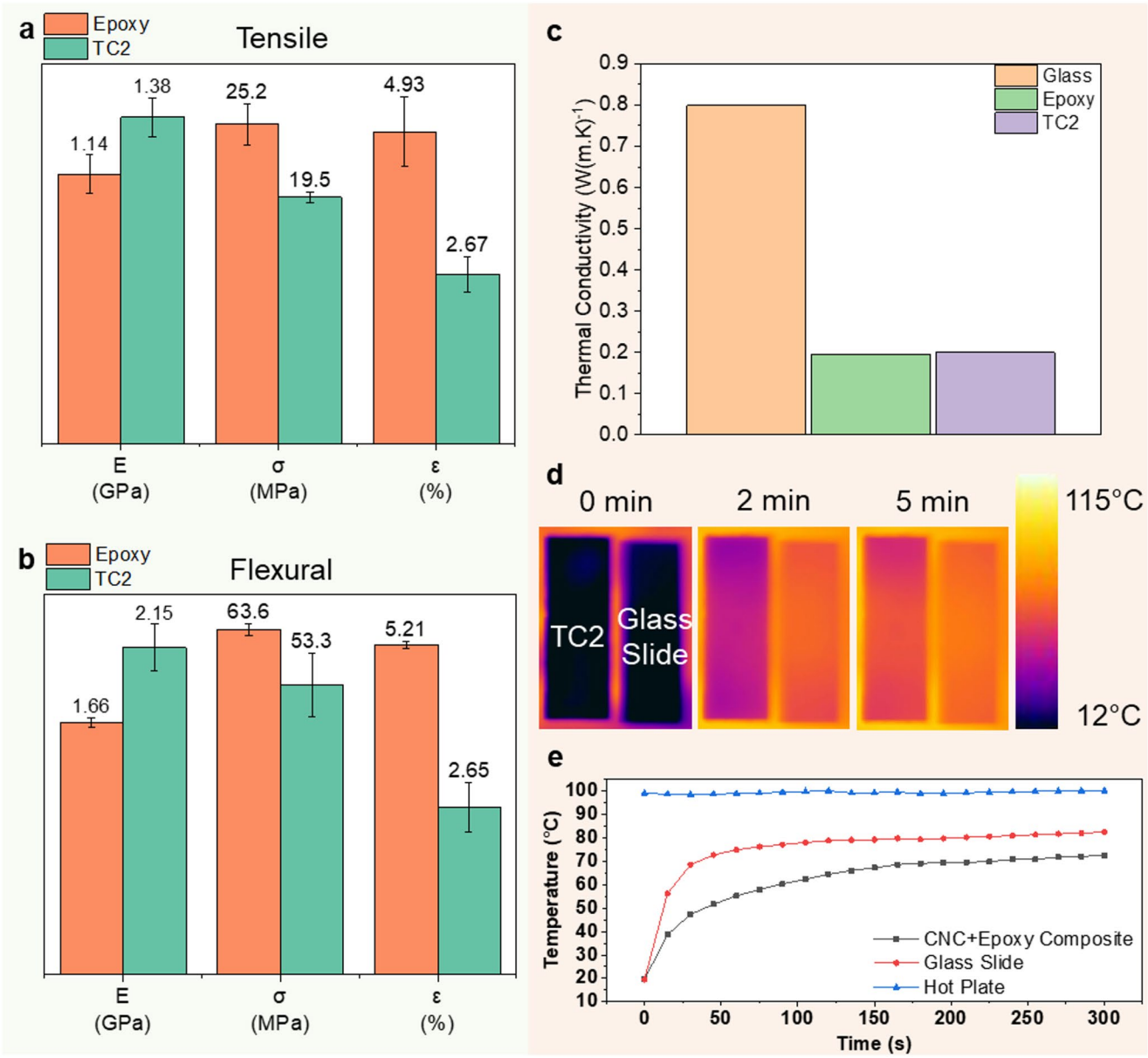

Fig. 3 Comparison of the mechanical and thermal properties of the TC2. (**a**) Elastic modulus (E), strength (σ), and strain at break (ε) for tensile tests. (**b**) Flexural modulus (E), strength (σ), and strain at break (ε) for 3-point-bending tests. (**c**) Thermal conductivity of TC2, pure epoxy and glass. (**d**) IR image and (**e**) temperature curve of the top surface of TC2 and glass slides placed on top of a hot plate at 100°C

increase in the flexural strength, too. The difference in the flexural strength of our TC2 and their TWs is attributed to their improved fabrication method which also involves a surface acetylation of the delignified wood substrate before the infiltration of PMMA. The authors confirm that the acetylation process improves compatibility between wood template and PMMA, leading to reduced interface debonding. The average strain at break values after the 3-point-bending tests were measured as 5.21% for pure epoxy and 2.65% for TC2. Typical stress-strain curves of TC2 and pure epoxy samples obtained after tensile and 3-point-bending tests are also provided in Figure S5.

The low thermal conductivity of TWs combined with the optical transparency has emerged their potential as energy efficient alternatives for glass in buildings [7, 15, 20, 21] and solar cell assemblies [1]. To show that our TCs are also good candidates for such applications, we performed a thermal conductivity measurement. As seen in Fig. 3c, the thermal conductivity of TC2 was measured as ~ 0.20 $W \cdot (m \cdot K)^{-1}$ while the thermal conductivity of the pure epoxy was ~ 0.19 $W\,(m\,K)^{-1}$. As given in Fig. 3d-e, we further performed studies to visualize the difference in the thermal conductivity of the TC2 and glass. After fabricating a TC2 sample having the exact dimensions with common glass slides (75 × 25 × 1

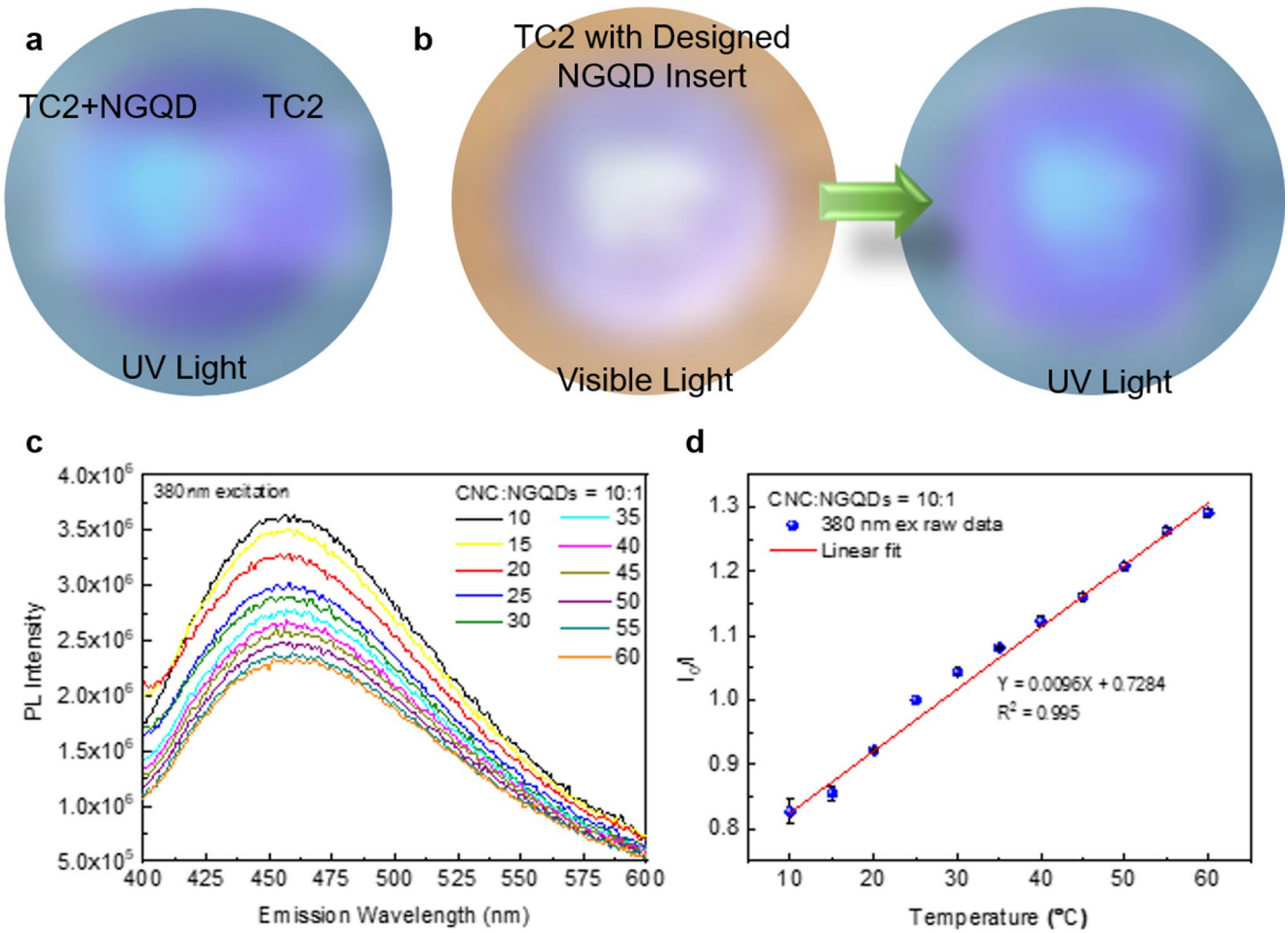

Fig. 4 Functionalization of TCs with graphene quantum dots. (**a**) TC2+NGQD and TC2 samples under UV light. (Anonymized) (**b**) TC2 sample with a designed NGQD insert under daylight and UV light. (Anonymized) (**c**) Temperature dependent photoluminescence of TC2+NGQD sample. (**d**) Photoluminescence intensity variation of TC2+NGQD sample as a function of temperature at an excitation wavelength of 380 nm

mm), both were placed on top of a hot plate at 100°C. While the temperature of the top surface of the glass reached and stabilized at ~ 80°C after 5 min, the top surface temperature of the TC2 sample remained at ~ 65°C. This showed that the CNC embedded inside the epoxy matrix didn't have a major impact on the thermal conductivity of the polymer matrix and hence, the much lower thermal conductivity of the TCs compared to glass makes them promising materials for the listed applications above.

Li et al. previously reported luminescent TWs potentially to be used in applications like furniture for general lighting, or luminescent solar concentrators for building integration [10]. Luminescence without causing a degradation in the optical transparency was obtained by doping the infiltrated polymer with different quantum dots (QDs). Unfortunately, their top-down fabrication approach does not allow a control on the location of the luminescent sections on the transparent composites which could further extend the use of luminescent TWs in applications such as smart displays [22]. Using our bottom-up fabrication approach, multiple print-heads, and adding a weighted amount of nitrogen-doped graphene quantum dot (NGQD) into the CNC ink, we were able to achieve TCs having designed luminescence characteristics. We synthesized NGQD based on another work [23] and used it as the functional additive for our TCs. MicroRaman spectrum, PL map, TEM images and average size distribution of the used NGQDs are presented in Figure S6. As presented in Figure S7a, while both CNC and CNC+NGQD aerogels do not have a noticeable difference under visible light, they are highly distinguishable under the UV light due to the luminescence of the NGQDs (Figure S7b). As given in Figure S7c, incorporating multiple print-heads can be used to obtain complex and designed geometries with different luminescence behavior. After infiltrating the epoxy, we were able to obtain luminescence and highly transparent TC2 + NGQD samples as presented in Fig. 4a. The optical transmission values of TC2 and TC2 + NGQD samples were also provided in Figure S8. Our bottom-up

approach enables a unique capability of manufacturing TCs with complex and designed luminescence as seen in Fig. 4b. As presented, the logo of our university was embedded inside the TC2 sample. While the logo is not visible under the visible light, exposing the sample to the UV light reveals the logo.

Yang et al. previously reported wide range (25–100°C) temperature sensors based on NGQDs due to their highly dependent photoluminescence (PL) intensity characteristics on the temperature [24]. To demonstrate the multifunctional nature of our TCs, we further evaluated the temperature sensing performance of our TC2 + NGQD composites using different CNC: NGQD ratios and excitation wavelengths. As seen in Figure S9, the highest linearity was obtained at the 385 nm excitation wavelength and the TC2-NGQD composite having the CNC: NGQD ratio of 10:1. As given in Fig. 4c, we have simultaneously measured the PL intensity of our composites under different temperatures. Similar to the observations of Yang et al., increasing temperature causes a continuous decrease in the PL intensity. As shown in Fig. 4d, the change in the intensity at the wavelength of 380 nm has almost a linear relation with the temperature with $R^2 = 0.995$. These results clearly show the feasibility of our multifunctional TC2-NGQD composites for temperature sensing applications.

4 Conclusion

In summary, based on our previous work on 3D printed functional aerogels, we propose a novel bottom-up approach for fabrication of multifunctional transparent composites similar to transparent wood. The proposed approach can enable precise patterning of the optical properties as well as other functionalities that can provide significant freedom in the device design. Furthermore, unlike the conventional top-down fabrication approach for transparent wood composites, our method can open a way to use eco-friendly bacterial cellulose instead of natural trees as the starting material. We expect that our novel fabrication approach can yield cost-efficient fabrication of functional optical devices that could be potentially used in applications such as gradient refractive index lenses, sensing devices, smart windows and screen applications.

Supplementary Information The online version contains supplementary material available at https://doi.org/10.1007/s40964-026-01570-6.

Author contributions DL designed and coordinated the study. HT, DK, and WHC performed experiments and characterizations. HT and DK prepared figures. HT wrote the manuscript with the input from all authors. All authors reviewed and commented on the manuscript.

Data availability No datasets were generated or analysed during the current study.

Declarations

Conflict of interest The authors declare no competing interests.

References

1. Li Y et al (2019) Optically transparent wood substrate for perovskite solar cells. ACS Sustain Chem Eng 7:6061–6067
2. Zhu M et al (2016) Highly Anisotropic, highly transparent wood composites. Adv Mater Deerfield Beach Fla 28:5181–5187
3. Fink S (1992) Transparent wood – A new approach in the functional study of wood structure. 46:403–408
4. Li Y, Vasileva E, Sychugov I, Popov S, Berglund L (2018) Optically transparent wood: recent Progress, opportunities, and challenges. Adv Opt Mater 6:1800059
5. Li Y, Fu Q, Yang X, Berglund L (2017) Transparent wood for functional and structural applications. Philos Trans R Soc Math Phys Eng Sci 376:20170182
6. Laboratory, U.S. (1987) The Laboratory, (), F. P. *Wood Handbook: Wood as an Engineering Material*
7. Li Y et al (2017) Lignin-Retaining Transparent Wood ChemSusChem 10:3445–3451
8. Xia Q et al (2021) Solar-assisted fabrication of large-scale, patternable transparent wood. Sci Adv 7:eabd7342
9. Ma L et al (2020) Bacterial cellulose: an encouraging eco-friendly nano-candidate for energy storage and energy conversion. J Mater Chem A 8:5812–5842
10. Li Y et al (2017) Luminescent transparent wood. Adv Opt Mater 5:1600834
11. Wang L, Liu Y, Zhan X, Luo D, Sun X (2019) Photochromic transparent wood for photo-switchable smart window applications. J Mater Chem C 7:8649–8654
12. Bisht P, Pandey KK, Barshilia HC (2021) Photostable transparent wood composite functionalized with an UV-absorber. Polym Degrad Stab 189:109600
13. Van Hai L et al (2023) Fabrication of eco-friendly transparent wood for UV-shielding functionality. Ind Crops Prod 201:116918
14. Yu Z et al (2017) Transparent wood containing CsxWO3 nanoparticles for heat-shielding window applications. J Mater Chem A 5:6019–6024
15. Montanari C, Li Y, Chen H, Yan M, Berglund LA (2019) Transparent wood for thermal energy storage and reversible optical transmittance. ACS Appl Mater Interfaces 11:20465–20472
16. Rahbar M, Han M, Xu S, Zobeiri H, Wang X (2023) Development of differential thermal resistance method for thermal conductivity measurement down to microscale. Int J Heat Mass Transf 202:123712
17. Scotti KL, Dunand DC (2018) Freeze casting – A review of processing, microstructure and properties via the open data repository, FreezeCasting.net. Prog Mater Sci 94:243–305
18. Nelson I, Naleway SE (2019) Intrinsic and extrinsic control of freeze casting. J Mater Res Technol 8:2372–2385
19. Shahbazi M-A, Ghalkhani M, Maleki H (2020) Directional Freeze-Casting: A bioinspired method to assemble multifunctional aligned porous structures for advanced applications. Adv Eng Mater 22:2000033
20. Li Y et al (2018) Towards centimeter Thick transparent wood through interface manipulation. J Mater Chem A 6:1094–1101
21. Mi R et al (2020) Scalable aesthetic transparent wood for energy efficient buildings. Nat Commun 11:3836

22. Okahisa Y, Yoshida A, Miyaguchi S, Yano H (2009) Optically transparent wood–cellulose nanocomposite as a base substrate for flexible organic light-emitting diode displays. Compos Sci Technol 69:1958–1961
23. Kurniawan D, Chiang W-H (2020) Microplasma-enabled colloidal nitrogen-doped graphene quantum Dots for broad-range fluorescent pH sensors. Carbon 167:675–684
24. Yang Y et al (2021) Multifunctional N-doped graphene quantum Dots towards Tetracycline detection, temperature sensing and high-performance WLEDs. J Photochem Photobiol Chem 405:112977